

# Nonperturbative Bethe–Heitler pair creation in combined high- and low-frequency laser fields

Sven Augustin<sup>a,b,\*</sup>, Carsten Müller<sup>a,b</sup>

<sup>a</sup>*Institut für Theoretische Physik I, Heinrich-Heine-Universität Düsseldorf, Universitätsstr. 1, 40225 Düsseldorf, Germany*

<sup>b</sup>*Max-Planck-Institut für Kernphysik, Saupfercheckweg 1, 69117 Heidelberg, Germany*

## Abstract

The nonperturbative regime of electron-positron pair creation by a relativistic proton beam colliding with a highly intense bichromatic laser field is studied. The laser wave is composed of a strong low-frequency and a weak high-frequency mode, with mutually orthogonal polarization vectors. We show that the presence of the high-frequency field component can strongly enhance the pair-creation rate. Besides, a characteristic influence of the high-frequency mode on the angular and energy distributions of the created particles is demonstrated, both in the nuclear rest frame and the laboratory frame.

**Keywords:** assisted, nonperturbative, nonlinear, Bethe–Heitler, pair creation, bichromatic, two-color, laser fields

**PACS:** 12.20.Ds, 32.80.Wr, 34.50.Rk, 42.50.Ct

## 1. Introduction

In the presence of very strong electromagnetic fields, the quantum vacuum can decay into electron-positron pairs [1, 2]. Pair creation in a constant electric field was studied in detail by Schwinger [3], employing the then newly established methods of quantum electrodynamics (QED). The resulting pair-creation rate has the form  $R \sim \exp(-\pi \mathcal{E}_{\text{cr}}/\mathcal{E})$ , where  $\mathcal{E}$  is the applied field and  $\mathcal{E}_{\text{cr}} = m^2/e$  the critical field of QED. Here,  $e = |e|$  and  $m$  are the positron charge and mass, respectively, and relativistic units with  $\hbar = c = 1$  are used. The Schwinger rate has a manifestly nonperturbative character due to its non-analytic field dependence. Therefore, it is of fundamental importance for our understanding of nonperturbative quantum field theories. An experimental verification has so far been prevented, though, by the huge value of  $\mathcal{E}_{\text{cr}} = 1.3 \times 10^{16}$  V/cm, which is not accessible in the laboratory yet.

The recent progress in high-intensity laser devices has strongly revived the interest in Schwinger pair creation.<sup>1</sup> In particular, various schemes have been proposed to facilitate its observation. Among them is a dynamically assisted variant where a rapidly oscillating electric field is superimposed onto a slowly varying electric field [6]. The total rate for pair creation in this field combination was shown to be strongly enhanced, while preserving its nonperturbative character. This interesting prediction has led to a number of subsequent investigations. Currently, the momentum distributions of pairs created by the dynamically assisted mechanism are under active scrutiny [7–9].

Pair-creation phenomena resembling the Schwinger effect can also occur when a beam of charged particles collides with a

counterpropagating intense laser beam. For instance, pair creation has been theoretically predicted in relativistic proton-laser collisions via a strong-field version of the Bethe–Heitler effect (see, e.g., [10–16]). When the laser frequency  $\omega$  is relatively small, so that the dimensionless parameter  $\xi \equiv e\mathcal{E}/m\omega$  becomes large,  $\xi \gg 1$ , the total rate for this process adopts the form  $R \sim \exp(-2\sqrt{3}\mathcal{E}_{\text{cr}}/\mathcal{E}')$  [13]. Here,  $\mathcal{E}' = (1 + \beta)\gamma\mathcal{E}$  denotes the laser field amplitude transformed to the rest frame of the proton, which is assumed to be sub-critical:  $\mathcal{E}' \ll \mathcal{E}_{\text{cr}}$ . The proton Lorentz factor  $\gamma$  and reduced velocity  $\beta$  have been introduced here. The similarity with the Schwinger rate is due to the fact that the characteristic length scale of pair creation in this parameter regime is much shorter than the laser wavelength, so that the field appears as quasi-static during the process.

An experimental setup to observe the strong-field Bethe–Heitler process could, in principle, be realized by utilizing the highly relativistic proton beam of the Large Hadron Collider (LHC) at CERN ( $\gamma \sim 7000$ ) in conjunction with a counter-propagating high-intensity laser beam ( $\mathcal{E} \sim 10^{11}$  V/cm). In fact, a very similar scheme was employed to observe pair creation by multiphoton absorption at the Stanford Linear Accelerator Center, where a 46 GeV electron beam colliding with an intense optical laser pulse triggered the pair creation [17]. This experiment, however, did not probe the Schwinger regime of pair creation because the field intensity was somewhat too low ( $\xi \approx 0.3$ ). Instead, the measured pair-creation rate showed a power-law dependence on the field strength.<sup>2</sup> Note that, a rate of the form  $R \sim \xi^{2n}$ , with  $n$  denoting the number of absorbed laser photons, follows from a consideration within the  $n$ -th order of perturbation theory, which is valid for  $\xi \ll 1$ .

Also for the strong-field Bethe–Heitler process, a dynamically

\*Corresponding author

Email addresses: sven.augustin@mpi-hd.mpg.de (Sven Augustin), carsten.mueller@tp1.uni-duesseldorf.de (Carsten Müller)

<sup>1</sup>For recent work on the Schwinger effect, see [4, 5] and references therein.

<sup>2</sup>However, an onset of nonperturbative signatures has been observed in [17]; see also [18].

assisted variant has been studied recently [19, 20]. There, it has been shown that the total pair-creation rates in relativistic proton-laser collisions may be strongly enhanced when a weak high-frequency component is superimposed onto an intense optical laser beam. Moreover, similar enhancement effects have been obtained for pair creation by the strong-field Breit–Wheeler process [21] and in spatially localized fields [22].

In this letter, we study strong-field Bethe–Heitler pair creation in a laser field consisting of a strong low-frequency and a weak high-frequency component. An  $\mathcal{S}$ -matrix calculation within the framework of laser-dressed QED employing Dirac–Volkov states is performed. Besides total pair-creation rates, our method allows us to calculate angular and energy distributions of the created particles that are not accessible to the polarization operator approach used in [19, 20]. The nonperturbative interaction regime with  $\xi \approx 1$  is analyzed both in the laboratory and the nuclear rest frame. We note that Bethe–Heitler pair creation in bichromatic laser fields has been studied recently, with a focus on interference and relative phase effects arising in the case of commensurable frequencies [23–25].

It is interesting to note that analogies of the Schwinger effect exist in other areas of physics. They have been demonstrated in various systems such as graphene layers in external electric fields [26], ultracold atom dynamics [27], and light propagation in optical lattices [28]. In these systems, the transition probability between quasiparticle and hole states shows Schwinger-like properties.

## 2. Theoretical Framework

Employing the  $\mathcal{S}$ -matrix formalism of electron-positron pair creation in combined laser and Coulomb fields, we write the transition amplitude in the nuclear rest frame as [10–12]

$$\mathcal{S} = i e \int \bar{\Psi}_{p_-, s_-}^{(-)} \gamma_0 A_N(r) \Psi_{p_+, s_+}^{(+)} d^4x. \quad (1)$$

Electron and positron are created with free momenta  $p_{\pm}$  and spins  $s_{\pm}$ , where the subscripted sign denotes their respective charge. They are described by relativistic Volkov states  $\Psi_{p_{\pm}, s_{\pm}}^{(\pm)}$  taking their interaction with a plane-wave laser field fully into account. In our case, this laser field is a superposition of two independent modes with the combined vector potential:

$$\mathbf{A}_L = \sum_{i=1,2} \mathbf{a}_i \cos(\eta_i), \quad (2)$$

wherein the phase variables  $\eta_i = x_{\mu} k_i^{\mu} = \omega_i t - \mathbf{k}_i \cdot \mathbf{r}$  are defined via the wave vectors  $k_i = \omega_i \kappa$ , where  $\kappa = (1, 0, 0, 1)$ . The individual amplitude vectors  $\mathbf{a}_i$  are chosen to be perpendicular and their absolute value is given by the dimensionless intensity parameters

$$\xi_i = \frac{e |\mathbf{a}_i|}{m \sqrt{2}}. \quad (3)$$

The nuclear Coulomb field  $A_N(r) = Ze/r$ , with the nuclear charge number  $Z$ , is treated in the lowest order of perturbation theory.

The  $\mathcal{S}$ -matrix may be evaluated by expanding the occurring periodic functions into Fourier series. The thereby introduced series summation indices  $n_i$ , with  $i = 1$  or  $2$ , may be understood as numbers of photons taken from the respective laser mode  $i$ . This expansion allows to perform the four-dimensional integration from Eq. (1) analytically by using the Fourier transform of the Coulomb potential and a representation of the  $\delta$ -function for the integral in space and time, respectively [29]:

$$\int d^4x A_N(r) \exp(i x_{\mu} Q^{\mu}) = \frac{4\pi Ze}{Q^2} 2\pi \delta(Q_0), \quad (4)$$

where  $Q = q_+ + q_- - n_1 k_1 - n_2 k_2$  is the momentum transfer to the nucleus and

$$q_{\pm} = p_{\pm} + \frac{e^2 \overline{\mathbf{A}_L^2}}{2\kappa_{\mu} p_{\pm}^{\mu}} \kappa \quad (5)$$

are the laser-dressed momenta. Note that, by definition of  $Q_0$ , the arising  $\delta$ -function ensures energy conservation.

The fully differential pair-creation rate is obtained by summing the square of the amplitude  $\mathcal{S}$  over the final spin states:

$$d^6 R = \frac{1}{T} \sum_{s_+, s_-} |\mathcal{S}|^2 \frac{d^3 q_-}{(2\pi)^3} \frac{d^3 q_+}{(2\pi)^3}, \quad (6)$$

where the time interval  $T$  has been introduced. For incommensurable frequencies, the squared  $\mathcal{S}$ -matrix adopts the form

$$|\mathcal{S}|^2 \sim \sum_{n_1, n_2} |M_{n_1, n_2}|^2 \delta(Q_0) T, \quad (7)$$

with the matrix element  $M_{n_1, n_2}$  containing the Fourier series coefficients.

For the following discussion, it will be particularly convenient to rewrite Eq. (6) by introducing *partial rates* distinguished by a single summation index, such that

$$d^6 R = \sum_{n_1} d^6 R_{n_1}, \quad (8)$$

$$d^6 R_{n_1} \sim \sum_{n_2} \sum_{s_+, s_-} |M_{n_1, n_2}|^2 \delta(Q_0) \frac{d^3 q_-}{(2\pi)^3} \frac{d^3 q_+}{(2\pi)^3}. \quad (9)$$

The  $\delta$ -function introduced in Eq. (4), allows to perform one integration analytically. In order to gain total rates or rates differential in a single coordinate the necessary remaining integrations are then calculated numerically.

## 3. Results

### 3.1. Total Pair-Creation Rates

In the following we shall apply our formalism to pair creation by a relativistic nuclear beam and a bichromatic laser field, which is composed of a high-frequency low-intensity (i.e., weak) mode ( $\omega_1 \sim 2m$ ,  $\xi_1 \ll 1$ ) and a low-frequency high-intensity (i.e., strong) mode ( $\omega_2 \ll 2m$ ,  $\xi_2 \sim 1$ ). Such a field may be achieved experimentally by the following combination in

the laboratory frame (primed): The assisting photon from the weak field with  $\omega'_1 = 70$  eV may be provided by an extreme-ultraviolet (XUV) source, e.g., one based on High-Harmonic Generation (HHG) [30] or a Free-Electron Laser (FEL) [31]. For the strong field, the 1064 nm infrared (IR) light emitted by an Nd:YAG (neodymium-doped yttrium aluminum garnet) laser may be frequency doubled in order to deliver  $\omega'_2 = 2.33$  eV. This corresponds to a frequency ratio of  $\omega_1/\omega_2 \approx 30$ . In combination with a proton beam of  $\gamma \lesssim 7460$ , as currently provided by the LHC [32], a setup of technology available today is feasible. Specifically, we will first examine the case of  $\gamma = 6600$ , with the resulting photon energies in the nuclear rest frame  $\omega_1 = 924$  keV and  $\omega_2 = 30.76$  keV, as well as  $\xi_1 = 1.45 \times 10^{-8}$ . Note that, the nuclear rest frame energy of the assisting mode is indicated by the notion of a  $\gamma$ -assisted process. Furthermore, the parameters of the assisting mode correspond to an intensity of approximately  $10^7$  W/cm<sup>2</sup> in the laboratory frame. We point out that this is a moderate value given the fact that present-day HHG and FEL sources may reach field intensities of the order of  $10^{13}$  W/cm<sup>2</sup> [33] and  $10^{18}$  W/cm<sup>2</sup> [34], respectively.

We shall begin with the comparison of strong-field Bethe-Heitler pair creation with and without the assistance of a single high-energetic photon. The respective total pair-creation rates  $R_{n_1}$  are shown in Fig. 1(a) for the nuclear rest frame. The corresponding rate in the laboratory frame is given by  $R'_{n_1} = R_{n_1}/\gamma$ . Even though the depicted intensity range of the strong mode is  $\xi_2 \approx 1$ , the total rates of both processes show a Schwinger-like dependence on this parameter:

$$R \sim \exp\left(-\frac{C}{\xi_2}\right). \quad (10)$$

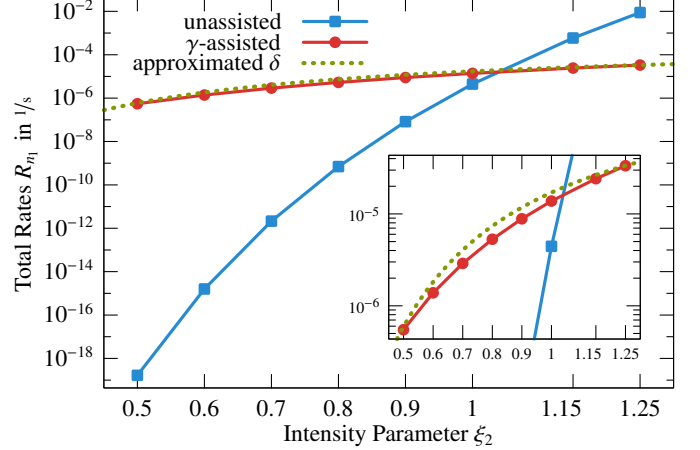
However, the coefficient  $C$  differs for the two cases. In the assisted process  $C$  is smaller, leading to an almost flat curve, while in the unassisted case a steep increase is visible.

Taking the absolute height into account, the influence of the assisting photon on the total pair-creation rate becomes apparent: As long as the intensity of the highly intense laser is below  $\xi_2 \approx 1$ , the assisted process shows a strong enhancement over the unassisted counterpart. However, from  $\xi_2 \approx 1$  onwards the situation inverts and the unassisted process becomes dominant.<sup>3</sup> Note that, the value of  $\xi_2$  where this crossing occurs may be influenced by adjusting  $\xi_1$ , on which the unassisted process does not depend and the assisted process depends quadratically. Therefore, a relative scaling between the two graphs is possible.

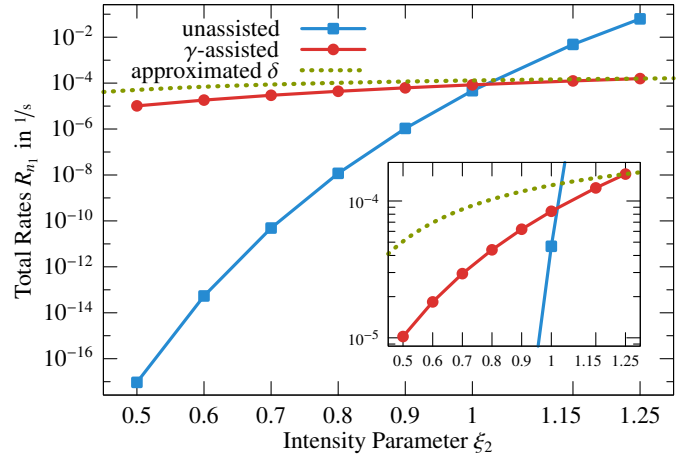
In a similar scheme, total rates of  $\gamma$ -assisted pair creation have been investigated fully analytically in [19]. Particularly, Eq. (9) therein (here quoted in a form adapted to our notation),

$$R \sim \exp\left(-\frac{2\sqrt{2}}{3\zeta}\right), \quad (11)$$

<sup>3</sup>Pair creation by the weak mode ( $\xi_1 = 1.45 \times 10^{-8}$ ,  $\omega_1 = 924$  keV) alone, without contribution from the strong mode (hence, for  $\xi_2 = 0$ ), is dominated by the absorption of two  $\omega_1$ -photons. We find a pair-creation rate of  $4.6 \times 10^{-17}$  1/s, which is much smaller than that of the respective dominating process in Fig. 1(a). The same is true for  $\omega_1 = 980$  keV, with a slightly larger rate of  $6.1 \times 10^{-17}$  1/s.



(a)  $\gamma = 6600$ ,  $\omega_1 = 924$  keV, and  $\omega_2 = 30.76$  keV



(b)  $\gamma = 7000$ ,  $\omega_1 = 980$  keV, and  $\omega_2 = 32.62$  keV

Figure 1: Total pair-creation rates of the unassisted and the  $\gamma$ -assisted process in the nuclear rest frame – For the latter, the result obtained here is compared to the analytical counterpart extracted from [19], as can be seen in the insets. For intensities below  $\xi_2 \approx 1$ , the assisted process dominates. Above this value, the situation inverts. In both figures,  $\xi_1 = 1.45 \times 10^{-8}$  is used.

with the parameters

$$\zeta = \frac{\chi}{\delta^{3/2}}, \quad \text{where} \quad \chi = \frac{1}{\sqrt{2}} \frac{\omega_2}{\omega_1} \xi_2, \quad (12)$$

$$\delta = \left(\frac{2m}{\omega_1}\right)^2 - 1 \approx \frac{2m - \omega_1}{m}, \quad (13)$$

allows for a comparison of the derived dependence on the strong field intensity  $\xi_2$  with our numerically integrated result. This comparison is done by scaling the exponential via a proportionality factor such that the values at  $\xi_2 = 1.25$  coincide. However, we note that Eq. (11) was obtained under the assumption that  $\xi_2 \gg 1$ . Even though this requirement is not met for the results shown in Fig. 1(a), where  $\xi_2 \sim 1$ , the additional graph – for the approximated  $\delta$  – shows very good agreement.

Besides this requirement of large intensities, there are two additional constraints demanded for the applicability of Eq. (11):

The two parameters given in Eq. (12) and Eq. (13) should be  $\ll 1$ . For the parameter set above, their values are both relatively small ( $\approx 0.2$ ) indeed. However, if we keep the laser combination in the laboratory fixed and increase  $\gamma$  to 7000, leading to photon energies in the nuclear rest frame of  $\omega_1 = 980$  keV and  $\omega_2 = 32.62$  keV, we end up with  $\zeta \approx 0.9$ . This expectedly leads to the significant deviation between our result and that obtained using Eq. (11) clearly visible in Fig. 1(b).

Had we chosen a  $\gamma$  lower than the initial 6600, the results would also have deviated from the prediction of Eq. (11), as then the parameter  $\delta$ , indicating the remaining energy gap that has to be overcome by absorption of photons from the strong laser mode ( $i = 2$ ), would have grown to and eventually overcome unity. Based on our results, we can establish an empirical extension to Eq. (11) valid for this regime. It has been obtained by expressing Eq. (11) in the form

$$R \sim \exp\left(-\frac{4}{3} \frac{1}{\omega_2} \omega_1 \left(2 - \frac{\omega_1}{m}\right)^{3/2} \frac{1}{\xi_2^d}\right), \quad (14)$$

where we have introduced an empirical fitting parameter  $d$ . Note that, for  $d$  set to unity, Eq. (14) is identical to Eq. (11) if the approximated expression for  $\delta$  from Eq. (13) is employed. Then we separately identified dependences on the two photon energies via fits to our results from a wide range of parameters,  $800 \text{ keV} \leq \omega_1 \leq 900 \text{ keV}$  and  $10 \text{ keV} \leq \omega_2 \leq 100 \text{ keV}$  in the nuclear rest frame, with according functions extracted from Eq. (14). From this we could gain that for  $d \approx 0.8$  the exponential scaling works well when  $\delta$  is not very small. While this is only a small deviation from the Schwinger-like form of Eq. (10), it can strongly impact the quantitative value of the predicted rates.

Note that, for the regime where the parameter  $\zeta$  is not very small, i.e., for energies of the assisting photon just below the pair-creation threshold like in Fig. 1(b), no constant empirical value for  $d$  could be determined, as the dependence on  $\xi_2$  changes rapidly with the precise value of the two parameters. This regime shall be further investigated in the subsequent section.

### 3.2. Angular- and Energy-Differential Spectra

Besides the total pair-creation rate, further insight into the differences between the assisted and the unassisted process may be found in the arising differential spectra. In particular, a potential experimental observation would rely on knowing the required acceptance of a detector and the optimal angle under which to measure.

Returning to the above parameter set with  $\gamma = 7000$ , where the parameter  $\zeta$  (cf. Eq. (12)) is relatively large, Fig. 2 shows the pair-creation rate differential in the emission angle  $\theta$  in the nuclear rest frame and the laboratory frame for the both processes at  $\xi_2 = 1$ , the approximate crossing point found in Fig. 1(b). The two key differences are the shifted peak position and the increased width of the distribution for the assisted process.

It is worth pointing out that, the minimal number of low-frequency photons to overcome the pair-creation threshold for the unassisted process in Fig. 2 amounts to  $n_2^{\min} = 45$ , whereas the assisted process requires only  $n_2^{\min} = 15$ . The difference between these threshold numbers corresponds to the frequency

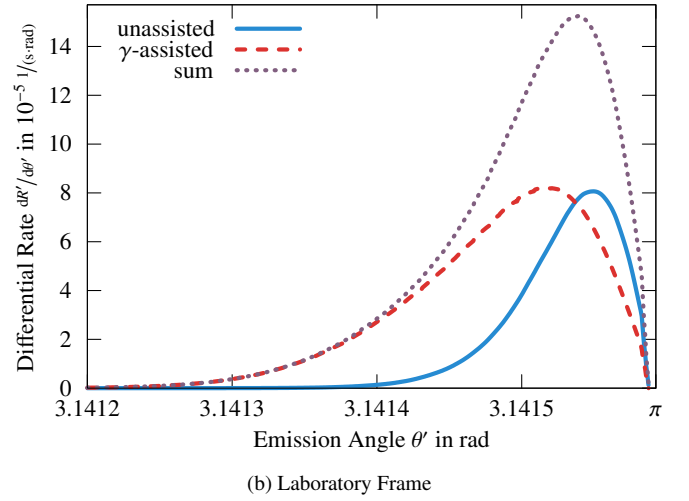
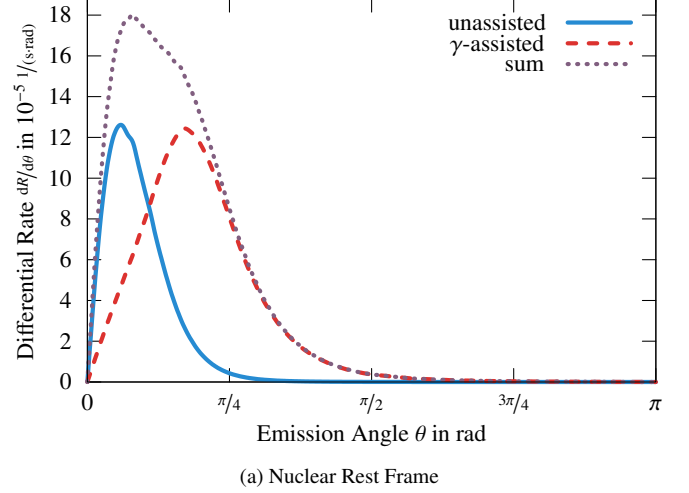
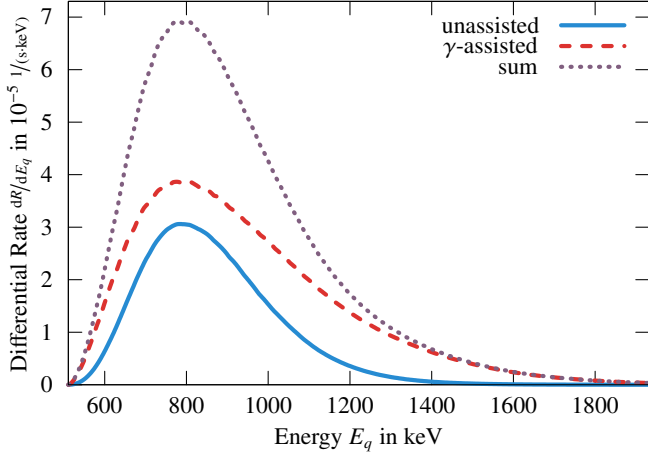


Figure 2: Angular-differential spectra of the unassisted and the  $\gamma$ -assisted process – The same parameters as in Fig. 1(b) have been used at  $\xi_2 = 1.0$ . In both frames of reference, the width of the distribution is increased for the assisted case. In the nuclear rest frame, the peak of the assisted process is shifted towards larger angles. Just as in the laboratory frame, towards slightly smaller angles.

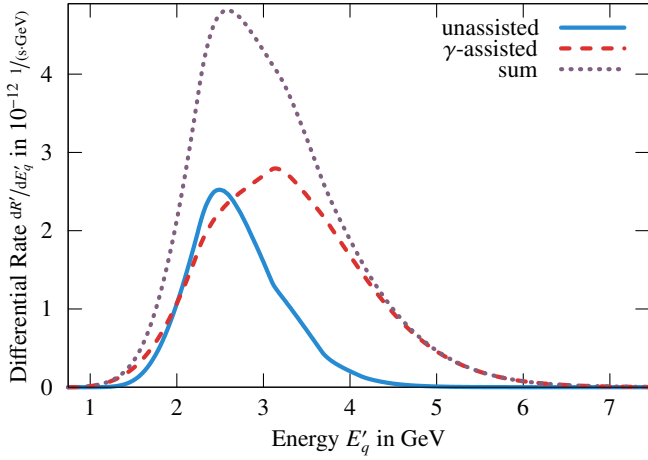
ratio  $\omega_1/\omega_2$ . The main contribution to the total pair-creation rates, though, stems from substantially larger photon numbers. For the unassisted process, the typical number  $n_2$  ranges from about 50 to 75, whereas it ranges from about 18 to 50 for the assisted process. Hence, the broader angular distribution arises in the case where the total number of absorbed photons is smaller. Interestingly, a similar effect of angular broadening for smaller photon numbers has also been found for pair creation by few-photon absorption in the perturbative interaction domain [35]. There, however, a small shift of the emission maximum towards larger angles has been found for larger photon numbers, in contrast to the present situation.

Note that, the Lorentz transformation contracts the full- $\pi$  spectrum of the nuclear rest frame (Fig. 2(a)) into a small range in the laboratory frame (Fig. 2(b)). Furthermore, it maps small angles





(a) Nuclear Rest Frame



(b) Laboratory Frame

Figure 3: Energy-differential spectra of the unassisted and the  $\gamma$ -assisted process – The same parameters as in Fig. 1(b) have been used at  $\xi_2 = 1.0$ . In both frames of reference, the width of the distribution is increased for the assisted case. In the nuclear rest frame the peak position remains unchanged, while it shifts towards larger energies in the laboratory frame.

to large angles and vice versa. Therefore, when comparing the distributions in one reference frame with its counterpart in the other, the spectra show a mirrored behavior. To both spectra, the summed-up differential rates  $dR/d\theta^{(r)}$ , with  $R = R_0 + R_1$  as defined in Eq. (8), have been added. Note that, the rate of the unassisted process could in principle be measured independently by turning off the assisting light source. In contrast, the assisted process occurs only simultaneously with its unassisted counterpart. Nevertheless, the distinction between the two processes in their contribution to the summed-up rate is more illustrative.

The energy distribution is depicted in Fig. 3 for the same parameters as above. Similar to Fig. 2, a broadening for the assisted process is found in both frames of reference. However, only in the laboratory frame the peak position is shifted. The latter may be attributed to the interweaving of the emission angle as given in Fig. 2(a) (contained in the  $z$ -component of the four-

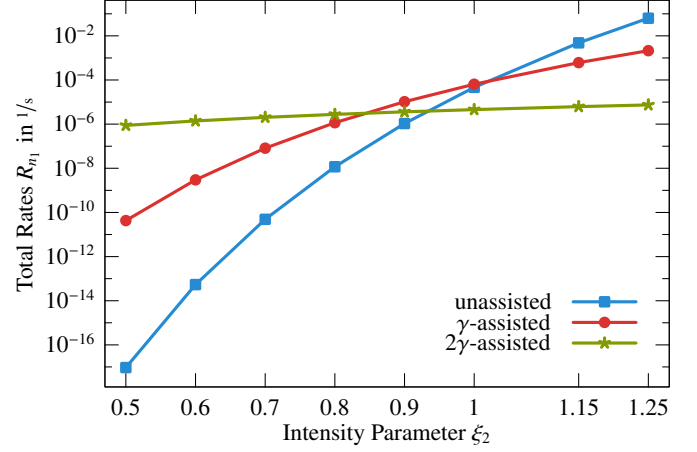


Figure 4: Total pair-creation rates of the unassisted, the singly  $\gamma$ -assisted, and the doubly  $\gamma$ -assisted process in the nuclear rest frame – With the parameters  $\omega_1 = 490$  keV,  $\omega_2 = 32.62$  keV, and  $\xi_1 = 1.45 \times 10^{-8}$ . For the smallest  $\xi_2$ , the doubly assisted process dominates. In an intermediate range,  $0.85 \lesssim \xi_2 \lesssim 1.02$ , the singly assisted process is strongest. Just as the unassisted process, for the highest  $\xi_2$ .

momentum) and the energy as given in Fig. 3(a) by the Lorentz transformation to the laboratory frame:

$$E'_q = \gamma(E_q + \beta q \cos(\theta)). \quad (15)$$

Hence, the peak position shift in the former manifests itself in the Lorentz-transformed version of the latter. Again, the summed-up rates  $dR/dE_q^{(r)}$  have been added to both spectra for the same reason as stated above.

### 3.3. Doubly $\gamma$ -Assisted Process

Extending our results to a higher-order assisted process may be straightforwardly done by halving  $\omega_1$ , the frequency of the assisting mode. This way we may compare the unassisted case (which obviously remains unchanged) to the assisted processes with one or two photons of high energy. Furthermore, the intensity of the assisting mode is increased to  $\xi_1 = 5 \times 10^{-5}$  to ensure better comparability of the three processes of interest. Besides, the parameters are identical to the above case of  $\gamma = 7000$ .

Analogous to Fig. 1, the total rates for these three processes are shown in Fig. 4 as function of  $\xi_2$ . We note that, in agreement with the above found behavior, for the lowest values of  $\xi_2$  the highest number of assisting photons, two, is dominant. From  $\xi_2 \approx 0.85$  onwards, the singly assisted process overgrows the former, which is in turn overgrown by the unassisted case for the highest depicted intensities ( $\xi_2 \gtrsim 1.02$ ).<sup>4</sup> It is worth pointing out that here, the singly  $\gamma$ -assisted process with  $\omega_1 = 490$  keV represents the aforementioned case where the parameter  $\delta$  (cf. Eq. (13)) is larger than unity, as  $\delta \approx 3.4$ .

<sup>4</sup>Here, pair-creation by the weak mode ( $\xi_1 = 5 \times 10^{-5}$ ,  $\omega_1 = 490$  keV) alone is dominated by the absorption of three  $\omega_1$ -photons, with a rate of  $2.6 \times 10^{-12} \text{ 1/s}$ .

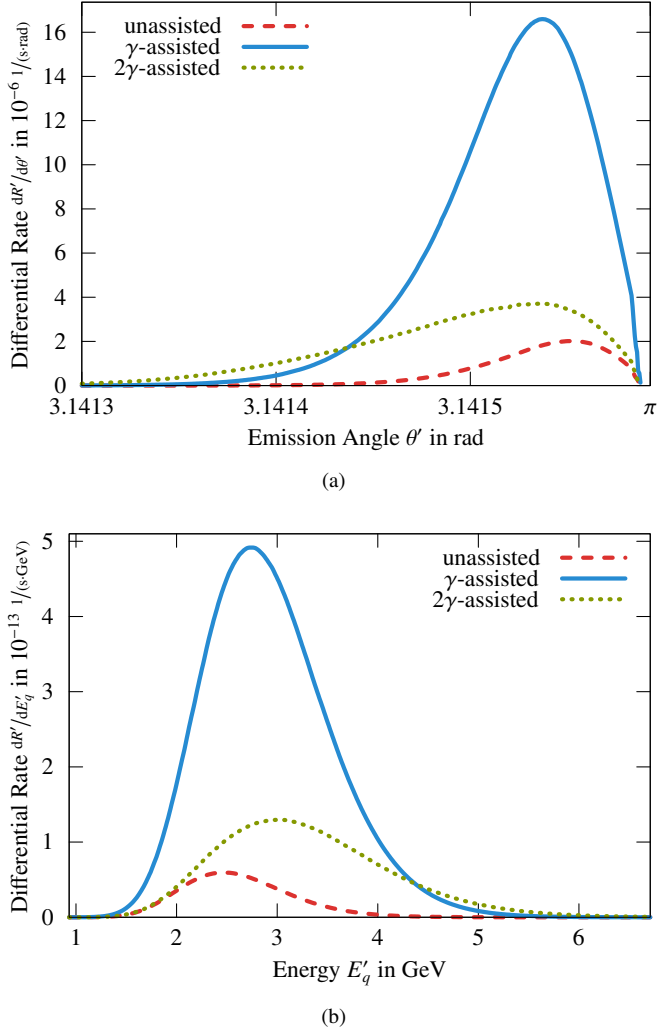


Figure 5: Differential spectra of the unassisted, the singly  $\gamma$ -assisted, and the doubly  $\gamma$ -assisted process in the laboratory frame – The same parameters as in Fig. 4 have been used at  $\xi_2 = 0.9$ . In accordance to Figs. 2 and 3, the width of both spectra is larger the more assisting photons are involved. Similarly, shifts of the peak position occur.

A similar agreement with the behavior found in Figs. 2 and 3 is visible for the angular and energy spectra depicted in Fig. 5 for  $\xi_2 = 0.9$ , where the three processes are of approximately equal strength. Evidently, the distributions are further widened and the peak position is shifted for the process with two assisting photons.

#### 4. Summary and Conclusion

We have studied the strong-field Bethe–Heitler process of electron-positron pair creation in relativistic proton-laser collisions, with the laser field consisting of a strong low-frequency and a weak high-frequency mode. Focusing on the nonperturbative interaction regime, where the intensity parameter of the strong mode is in the order of unity ( $\xi_2 \approx 1$ ), we have shown that the assistance of the high-frequency field component can largely

enhance the total pair-creation rate. The latter still exhibits a manifestly nonperturbative field dependence, similar to the famous Schwinger rate. This way we extended previous results valid for  $\xi_2 \gg 1$  [19, 20] to the intermediate laser-matter coupling regime and showed, moreover, that the field scaling of the Schwinger-like exponent changes significantly when the high laser frequency closely approaches the pair-creation threshold (in the proton rest frame).

Additionally, we have demonstrated that the  $\gamma$ -assisted pair-creation mechanism exerts a characteristic influence on the angular and energy distributions of created particles. It leads to shifts of the emission maxima and a broadening of the distributions. Finally, a regime of parameters has been identified where the assistance of two high-frequency photons strongly affects, or even dominates, the pair-creation rate. In accordance with the above, characteristic changes were also found in the underlying spectra.

Our results can be tested experimentally by combining the LHC proton beam with a counterpropagating laser pulse comprised of a highly intense optical mode and a high-frequency (XUV or soft X-ray) mode of moderate intensity.

#### Acknowledgments

Funding for this project by the German Research Foundation (DFG) under Grant No. MU 3149/1-1 is gratefully acknowledged. S.A. also wishes to thank the Heidelberg Graduate School of Fundamental Physics (HGSFP) for the generous travel support.

#### References

#### References

- [1] F. Sauter, Über das Verhalten eines Elektrons im homogenen elektrischen Feld nach der relativistischen Theorie Diracs, Z. Physik 69 (1931) 742–764. W. Heisenberg, H. Euler, Folgerungen aus der Diracschen Theorie des Positrons, Z. Physik 98 (1936) 714–732.
- [2] W. Greiner, B. Müller, J. Rafelski, Quantum Electrodynamics of Strong Fields, Springer, Berlin, Heidelberg, 1985.
- [3] J. Schwinger, On gauge invariance and vacuum polarization, Phys. Rev. 82 (1951) 664–679.
- [4] A. Ringwald, Pair production from vacuum at the focus of an X-ray free electron laser, Phys. Lett. B 510 (2001) 107–116. R. Ruffini, L. Vitagliano, S.-S. Xue, On plasma oscillations in strong electric fields, Phys. Lett. B 559 (2003) 12–19. S. S. Bulanov, V. D. Mur, N. B. Narozhny, J. Nees, V. S. Popov, Multiple colliding electromagnetic pulses: a way to lower the threshold of  $e^+ e^-$  pair production from vacuum, Phys. Rev. Lett. 104 (2010) 220404. C. K. Dumlu, G. V. Dunne, Stokes phenomenon and Schwinger vacuum pair production in time-dependent laser pulses, Phys. Rev. Lett. 104 (2010) 250402. F. Hebenstreit, R. Alkofer, H. Gies, Particle self-bunching in the Schwinger effect in spacetime-dependent electric fields, Phys. Rev. Lett. 107 (2011) 180403. C. Kohlfürst, M. Mitter, G. von Winckel, F. Hebenstreit, R. Alkofer, Optimizing the pulse shape for Schwinger pair production, Phys. Rev. D 88 (2013) 045028.
- [5] F. Ehlotzky, K. Krajewska, J. Z. Kamiński, Fundamental processes of quantum electrodynamics in laser fields of relativistic power, Rep. Prog. Phys. 72 (2009) 046401. A. Di Piazza, C. Müller, K. Z. Hatsagortsyan, C. H. Keitel, Extremely high-intensity laser interactions with fundamental quantum systems, Rev. Mod. Phys. 84 (2012) 1177–1228.

- [6] R. Schützhold, H. Gies, G. Dunne, Dynamically assisted Schwinger mechanism, *Phys. Rev. Lett.* 101 (2008) 130404. G. V. Dunne, H. Gies, R. Schützhold, Catalysis of Schwinger vacuum pair production, *Phys. Rev. D* 80 (2009) 111301.
- [7] M. Orzhaber, F. Hebenstreit, R. Alkofer, Momentum spectra for dynamically assisted Schwinger pair production, *Phys. Lett. B* 698 (2011) 80–85.
- [8] C. Fey, R. Schützhold, Momentum dependence in the dynamically assisted Sauter–Schwinger effect, *Phys. Rev. D* 85 (2012) 025004.
- [9] Z.-L. Li, D. Lu, B.-S. Xie, Multiple-slit interference effect in the time domain for boson pair production, *Phys. Rev. D* 89 (2014) 067701.
- [10] C. Müller, A. B. Voitkiv, N. Grün, Differential rates for multiphoton pair production by an ultrarelativistic nucleus colliding with an intense laser beam, *Phys. Rev. A* 67 (2003) 063407.
- [11] H. K. Avetissian, A. K. Avetissian, G. F. Mkrtchian, K. V. Sedrakian, X-ray free electron laser for electron-positron pair production on the nuclei, *Nucl. Instrum. Methods Phys. Res. Sect. A* 507 (2003) 582 – 586.
- [12] P. Siczka, K. Krajewska, J. Z. Kamiński, P. Panek, F. Ehlötzky, Electron-positron pair creation by powerful laser-ion impact, *Phys. Rev. A* 73 (2006) 053409.
- [13] A. I. Milstein, C. Müller, K. Z. Hatsagortsyan, U. D. Jentschura, C. H. Keitel, Polarization-operator approach to electron-positron pair production in combined laser and Coulomb fields, *Phys. Rev. A* 73 (2006) 062106.
- [14] M. Y. Kuchiev, D. J. Robinson, Electron-positron pair creation by Coulomb and laser fields in the tunneling regime, *Phys. Rev. A* 76 (2007) 012107.
- [15] T.-O. Müller, C. Müller, Spin correlations in nonperturbative electron-positron pair creation by petawatt laser pulses colliding with a TeV proton beam, *Physics Letters B* 696 (2011) 201–206.
- [16] F. Fillion-Gourdeau, E. Lorin, A. D. Bandrauk, Resonantly enhanced pair production in a simple diatomic model, *Phys. Rev. Lett.* 110 (2013) 013002.
- [17] D. L. Burke, R. C. Field, G. Horton-Smith, J. E. Spencer, D. Walz, S. C. Berridge, W. M. Bugg, K. Shmakov, A. W. Weidemann, C. Bula, K. T. McDonald, E. J. Prebys, C. Bamber, S. J. Boege, T. Koffas, T. Kotseroglou, A. C. Melissinos, D. D. Meyerhofer, D. A. Reis, W. Ragg, Positron production in multiphoton light-by-light scattering, *Phys. Rev. Lett.* 79 (1997) 1626–1629.
- [18] H. R. Reiss, Special analytical properties of ultrastrong coherent fields, *The European Physical Journal D* 55 (2009) 365–374. H. Hu, C. Müller, C. H. Keitel, Complete QED theory of multiphoton trident pair production in strong laser fields, *Phys. Rev. Lett.* 105 (2010) 080401.
- [19] A. Di Piazza, E. Lötstedt, A. I. Milstein, C. H. Keitel, Barrier control in tunneling  $e^+e^-$  photoproduction, *Phys. Rev. Lett.* 103 (2009) 170403.
- [20] A. Di Piazza, E. Lötstedt, A. I. Milstein, C. H. Keitel, Effect of a strong laser field on electron-positron photoproduction by relativistic nuclei, *Phys. Rev. A* 81 (2010) 062122.
- [21] M. J. A. Jansen, C. Müller, Strongly enhanced pair production in combined high- and low-frequency laser fields, *Phys. Rev. A* 88 (2013) 052125.
- [22] M. Jiang, W. Su, Z. Q. Lv, X. Lu, Y. J. Li, R. Grobe, Q. Su, Pair creation enhancement due to combined external fields, *Phys. Rev. A* 85 (2012) 033408. M. Jiang, Q. Z. Lv, Z. M. Sheng, R. Grobe, Q. Su, Enhancement of electron-positron pair creation due to transient excitation of field-induced bound states, *Phys. Rev. A* 87 (2013) 042503.
- [23] K. Krajewska, J. Z. Kamiński, Phase effects in laser-induced electron-positron pair creation, *Phys. Rev. A* 85 (2012) 043404.
- [24] S. P. Roshchupkin, Interference effect in the photoproduction of electron-positron pairs on a nucleus in the field of two light waves, *Phys. At. Nucl.* 64 (2001) 243–252.
- [25] S. Augustin, C. Müller, Interference effects in Bethe–Heitler pair creation in a bichromatic laser field, *Phys. Rev. A* 88 (2013) 022109. S. Augustin, C. Müller, Nonlinear Bethe–Heitler pair creation in an intense two-mode laser field, *J. Phys. Conf. Ser.* 497 (2014) 012020.
- [26] D. Allor, T. D. Cohen, D. A. McGady, Schwinger mechanism and graphene, *Phys. Rev. D* 78 (2008) 096009. G. L. Klimchitskaya, V. M. Mostepanenko, Creation of quasiparticles in graphene by a time-dependent electric field, *Phys. Rev. D* 87 (2013) 125011.
- [27] N. Szpak, R. Schützhold, Optical lattice quantum simulator for quantum electrodynamics in strong external fields: spontaneous pair creation and the Sauter–Schwinger effect, *New Journal of Physics* 14 (2012) 035001.
- [28] F. Dreisow, S. Longhi, S. Nolte, A. Tünnermann, A. Szameit, Vacuum instability and pair production in an optical setting, *Phys. Rev. Lett.* 109 (2012) 110401.
- [29] J. D. Bjorken, S. D. Drell, *Relativistic Quantum Mechanics*, McGraw-Hill, New York, 1964. In Sec. 7.1.
- [30] X. Zhang, A. L. Lytle, T. Popmintchev, X. Zhou, H. C. Kapteyn, M. M. Murnane, O. Cohen, Quasi-phase-matching and quantum-path control of high-harmonic generation using counterpropagating light, *Nat Phys* 3 (2007) 270–275.
- [31] W. Ackermann, G. Asova, V. Ayvazyan, A. Azima, N. Baboi, J. Bahr, V. Balandin, B. Beutner, A. Brandt, A. Bolzmann, R. Brinkmann, O. I. Brovko, M. Castellano, P. Castro, L. Catani, E. Chiadroni, S. Choroba, A. Cianchi, J. T. Costello, D. Cubaynes, Operation of a free-electron laser from the extreme ultraviolet to the water window, *Nat. Photon.* 1 (2007) 336–342.
- [32] O. S. Brüning, P. Collier, P. Lebrun, S. Myers, R. Ostojic, J. Poole, P. Proudlock, The LHC Main Ring, LHC Design Report I (2004).
- [33] H. Mashiko, A. Suda, K. Midorikawa, Focusing multiple high-order harmonics in the extreme-ultraviolet and soft-x-ray regions by a platinum-coated ellipsoidal mirror, *Appl. Opt.* 45 (2006) 573–577.
- [34] L. Young, E. P. Kanter, B. Krässig, Y. Li, A. M. March, S. T. Pratt, R. Santra, S. H. Southworth, N. Rohringer, L. F. DiMauro, G. Doumy, C. A. Roedig, N. Berrah, L. Fang, M. Hoener, P. H. Bucksbaum, J. P. Cryan, S. Ghimire, J. M. Glowina, D. A. Reis, J. D. Bozek, C. Bostedt, M. Messerschmidt, Femtosecond electronic response of atoms to ultra-intense X-rays, *Nature* 466 (2010) 56–61.
- [35] S. J. Müller, C. Müller, Few-photon electron-positron pair creation by relativistic muon impact on intense laser beams, *Phys. Rev. D* 80 (2009) 053014.